Evaluation of the surface bonding energy of an InP membrane bonded oxide-free to Si using instrumented nanoindentation

K. Pantzas, G. Patriarche, E. Le Bourhis, David Troadec, A. Itawi, G. Beaudoin, I. Sagnes, A. Talneau

Evaluation of the surface bonding energy of an InP membrane bonded oxide-free to Si using instrumented nanoindentation

Cite as: Appl. Phys. Lett. **103**, 081901 (2013); https://doi.org/10.1063/1.4817675
Submitted: 20 May 2013 • Accepted: 21 July 2013 • Published Online: 19 August 2013

Konstantinos Pantzas, Gilles Patriarche, Eric Le Bourhis, et al.

Evaluation of the surface bonding energy of an InP membrane bonded oxide-free to Si using instrumented nanoindentation

Konstantinos Pantzas,[1,2,a)] Gilles Patriarche,[1] Eric Le Bourhis,[2] David Troadec,[3] Ahmad Itawi,[1] Grégoire Beaudoin,[1] Isabelle Sagnes,[1] and Anne Talneau[1]
[1]*CNRS-LPN, Route de Nozay, F-91460, Marcoussis, France*
[2]*Institut P', CNRS-Université de Poitiers - ENSMA - UPR 3346, SP2MI - Téléport 2 Bd Marie Pierre Curie, B.P. 30179, F-86962, Futuroscope Chasseneuil CEDEX, France*
[3]*CNRS, Institut d'Electronique, de Microélectronique & de Nanotechnologie, UMR 8520, F-59652 Villeneuve Dascq, France*

(Received 20 May 2013; accepted 21 July 2013; published online 19 August 2013)

Instrumented nanoindentation is used in conjunction with scanning transmission electron microscopy to evaluate the mechanical resistance at the bonding interface of a 450 nm thick InP membrane bonded oxide-free to Si. Indentation using a Berkovich tip is shown to cause the planes in InP to rotate by as much as 16°. The shear stress resulting from this rotation causes the InP membrane to buckle, forming a debonded blister around the indented zone. The geometry of this blister is used to compute the surface bond energy of InP bonded oxide-free to Si. An average surface bonding energy of 585 mJ m^{-2} is reported. © *2013 AIP Publishing LLC*. [http://dx.doi.org/10.1063/1.4817675]

Over the past few years, direct bonding of highly mismatched semiconductors has been shown to be a promising alternative to hetero-epitaxy in the production of integrated photonic devices, opening the path for the fabrication of a whole new class of optoelectronic components. The bonding of indium phosphide (InP) to silicon (Si) ($\Delta a/a = 8.1\%$), for instance, allows the direct coupling of emission and/or amplification at 1.55 μm to silicon waveguides. Several approaches to direct bonding have been proposed in the literature: approaches using benzocyclobutene (BCB),[1] thick oxides,[2–6] thin oxides,[7] and, finally, no oxides[8,9] have been demonstrated.

In all of these approaches, the wafers to be bonded are brought together after careful surface preparation and are held together by Van der Waals forces. An annealing step is then implemented to form covalent bonds at the bonding interface. A common way to evaluate the quality of the reconstructed interface is to measure the surface bonding energy.[2] The surface bonding energy is usually measured using the crack-opening method.[2–4,10] In this method, a thin blade of thickness t_b is carefully inserted between the bonded wafers. This experiment creates a debonding crack of length L at the bonding interface. In the general case of two dissimilar wafers, the surface bonding energy γ relates to the debonding crack length L as follows:

$$\gamma = \frac{3t_b^2 E_1 t_{w1}^3 E_2 t_{w2}^3}{8L^4(E_1 t_{w1}^3 + E_2 t_{w2}^3)}, \quad (1)$$

where t_{wi} and E_i represent the thickness and the Young modulus of wafer i.

While this method has its merits, it requires the preparation of a dedicated specimen and gives a surface bonding energy for the average sample. Moreover, the razor-blade technique can only be applied after the annealing step described previously. In most applications, however, there are several fabrication steps after the annealing of the wafers, including, at least, the removal of one of the wafers, to leave only a thin membrane to be used in the final application. Finally, the reliability of the measurement given by the razor-blade method has been called into question,[5] as the crack length depends heavily on the experimental conditions, especially during the insertion of the razor blade.

In other fields of surface adhesion, such as the adhesion of coatings to glass, instrumented nanoindentation has been proven to be a reliable means of producing localized, reproducible, and highly sensitive measurements of the surface bonding energy of ultra-thin coatings to a substrate.[11–15] In a recent contribution, the authors proposed to apply instrumented nanoindentation to the case of InP bonded oxide-free to Si.[9] Indentation of the membrane at high loads revealed a characteristic pop-in at 80 mN. This second pop-in is distinct from the pop-in of elasto-plastic transition in InP, which is observed at 0.5 mN, and is present only in the InP membranes, and not in bulk InP. In this approach, however, this second pop-in load was shown to be associated with both lateral and radial cracks. Thus, one cannot straightforwardly associate this pop-in load with the surface bonding energy between the InP membrane and the Si substrate.

In the present study, the authors examine the case of indentation loads between 5 and 50 mN. In this intermediate regime, a blister is shown to form around the indented zone. Scanning transmission electron microscopy (STEM) is used to determine the mechanics of the blister formation to compute the surface bonding energy of the InP/Si system.

For the purpose of the present study, a 450 nm thick membrane of InP was grown on top of lattice-matched InGaAs etch-stop layer on an InP substrate using metal-organic chemical-vapor deposition (MOCVD). The surfaces of the MOCVD-grown InP and the Si samples were then carefully prepared to remove all traces of oxide. The samples were then immediately brought into contact and inserted in the wafer bonder, where they were annealed at 550 °C under vacuum for 90 min. The InP substrate and InGaAs layers were then chemically removed, leaving only the 450 nm thick

a)konstantinos.pantzas@lpn.cnrs.fr

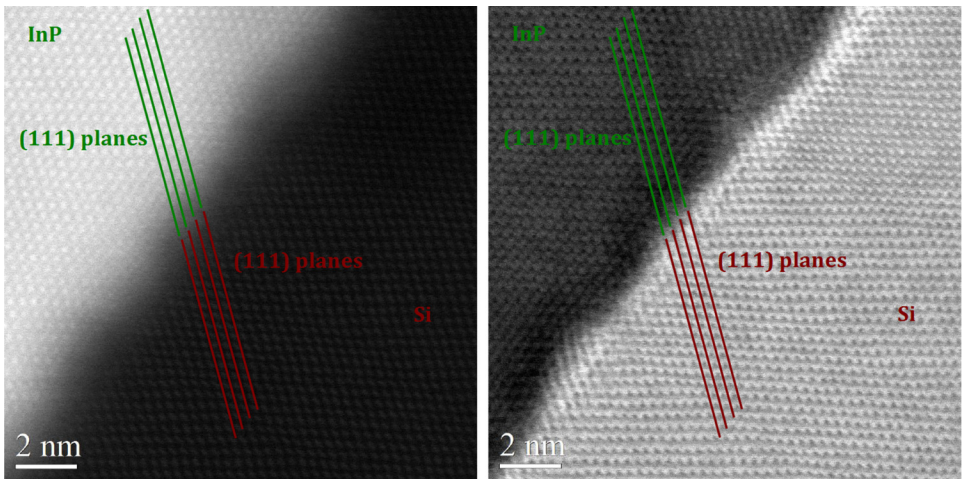

FIG. 1. Atomic-resolution HAADF (left) and BF (right) STEM images of the oxide-free bonding interface between InP and Si in the reference specimen.

MOCVD-grown InP membrane on the Si substrate. Further details on the bonding procedure can be found in Ref. 8.

The membrane was then deformed in a Nanohardness tester from CSEM using a Berkovich diamond tip. The calibration procedure suggested by Oliver and Pharr[16] was used to correct for the load-frame compliance of the apparatus and the imperfections of the shape of the indenter tip. Indentation loads of 5, 10, 20, and 50 mN were applied at different locations of the surface of the membrane. One STEM specimen per load was then prepared from the sample using Focused Ion Beam (FIB) etching. A fifth specimen was also prepared using FIB etching from an unindented region of the membrane, to serve as a reference.

Scanning transmission electron microscopy was then performed in an aberration-corrected JEOL 2200FS microscope, operating at 200 kV with a probe current of 150 pA, and a probe size of 0.12 nm at the full width at half maximum. The convergence half-angle of the probe was 30 mrad and the detection inner and outer half-angles for the high-angle annular dark field STEM (HAADF-STEM) images were 100 and 170 mrad, respectively. The specimens were imaged along the $\langle 110 \rangle$ zone axis.

Atomic-resolution HAADF-STEM and bright-field STEM (BF-STEM) images of the unindented reference specimen are shown in Figure 1. The interface between InP and Si is reconstructed over a few atomic planes. The images show the absence of any layer of oxide between InP and Si.

A low-magnification BF-STEM image of the specimen corresponding to a load of 10 mN is shown in Figure 2. The impression made by the indenter is outlined. The shape of the impression is asymmetric: the steeper left-hand side corresponds to a facet of the pyramid, while the right-hand side is the impression of the opposing edge. The region where one observes the dislocations generated by the indenter tip is also outlined. At low indentation loads (<50 mN), the dislocations generated by the indenter do not cross the interface between InP and Si and are contained within the InP membrane. The lateral extent of the region containing the dislocations is confined within a circle, the radius c of which can be estimated using the following equation:

$$c = \sqrt{\frac{3}{2\pi}\frac{F_{\max}}{Y}}, \qquad (2)$$

where $F_{\max}$ is the maximum indentation load used in the experiment and Y the representative flow stress of the indented layer.[17]

The BF-STEM in Figure 2 also reveals that the InP membrane forms a blister surrounding the dislocation-dense region close to the indenter a phenomenon known as buckling also reported to occur in the case of coatings on glass or silicon.[12–15] In this blister, the InP membrane is debonded from the Si substrate, but not plastically deformed. A closer inspection of the InP membrane beneath the indenter tip reveals that the origin of this debonding is the result of a macroscopic rotation of the planes of InP around $\langle 110 \rangle$ under the effect of the indenter. An example is given in the atomic-atomic resolution BF-STEM image of the interface between InP and Si presented in Figure 3. The image corresponds to the specimen indented with a maximum load of 16 mN. The $(1\ 1\ 1)$ and $(1\ \bar{1}\ 1)$ planes of InP and Si have been outlined for clarity. This rotation can be observed far from the apex of the indenter tip.

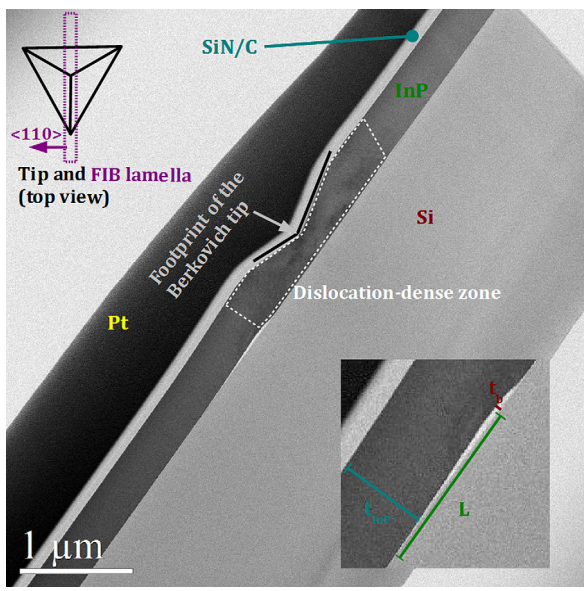

FIG. 2. Low-magnification BF-STEM image of the specimen indented with a maximum load of 10 mN. The impression made by the indenter is outlined on the image. Debonding can be observed far from the indented region. Inset shows an enlarged section of the image centered on the blister on the left-hand side of the indented region.

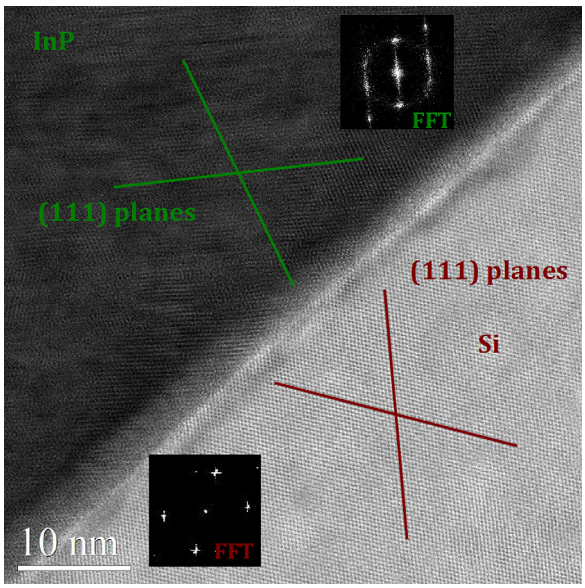

FIG. 3. Atomic-resolution BF-STEM image of the interface between InP and Si below the apex of the indenter. The outlined (1 1 1) and (1 $\bar{1}$ 1) planes of InP and Si reveal that the InP membrane macroscopically rotates during the indentation experiment. Insets show the Fourier transforms of the InP and Si layers.

The magnitude of the rotation was measured by applying the geometric phase analysis (GPA) algorithm[18] to atomic resolution images of the interface between Si and InP in the various specimen. The mapping of the rotation computed from the image shown in Figure 3 is presented in Figure 4. The InP layer in this case is shown to rotate by as much as 16° (Fig. 5). The magnitude of the rotation for the various loads explored is summarized in Table I.

This rotation can be explained as follows: for loads higher than 0.5 mN, mixed dislocations are generated in InP to accommodate the applied deformation. These dislocations

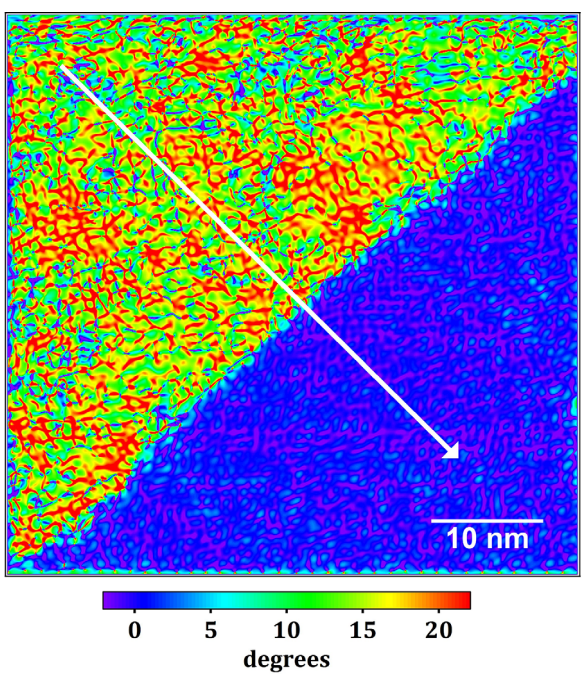

FIG. 4. Mapping of the rotation observed in Figure 3, obtained using the GPA algorithm.

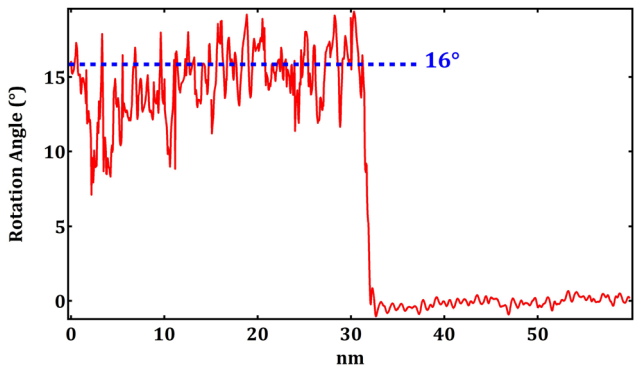

FIG. 5. Profile along the white arrow in Figure 4. The average rotation is 16°.

propagate along the (1 1 1) planes, until they reach the interface between InP and Si. The interface acts as a grain boundary, preventing the dislocations from propagating into the Si substrate. As a result of the asymmetry of the Berkovich tip relative to the InP lattice, more dislocations accumulate on the left-hand side of the tip (see Figure 6). The edge component of these dislocations causes the InP membrane to uniformly rotate around ⟨110⟩ until the torque is sufficient to debond the membrane from the Si substrate.

The above explanation can be verified by comparing the measured rotation, against the expected rotation, obtained from the following derivation. In the limit of small angles, the mean lateral spacing D between adjacent dislocations in a tilt grain boundary is given by[19]

$$D = \frac{b}{\theta}, \tag{3}$$

where b is the magnitude of edge component of the dislocations' Burgers vector and θ the angle by which the membrane has rotated. In the case of InP, this equation becomes

$$D = \frac{a_{\mathrm{InP}}}{\sqrt{2}\theta}. \tag{4}$$

At an applied load of 10 mN, the indenter has penetrated the membrane by 215 nm, and InP is displaced along the (1 1 1) planes. Under these conditions, the indenter is expected to generate approximately 4300 dislocations in the membrane. The dislocation-dense zone at the bonding interface extends by 2.2 μm at the same load, yielding an average spacing D of approximately 5 Å and, thus, an angle θ of 8°. This value is close to the measured average rotation for the same load.

TABLE I. Summary of findings.

Load mN	Rotation deg	Crack length μm	Blister height nm	Energy mJ m^{-2}
0 (ref.)	0	…	…	…
5	2	0.27	6.7	(n/a)[a]
10	8	0.99	23.4	594
20	16	1.66	61	511
50	0–30	1.4	49	651

[a]Calculation not applicable.

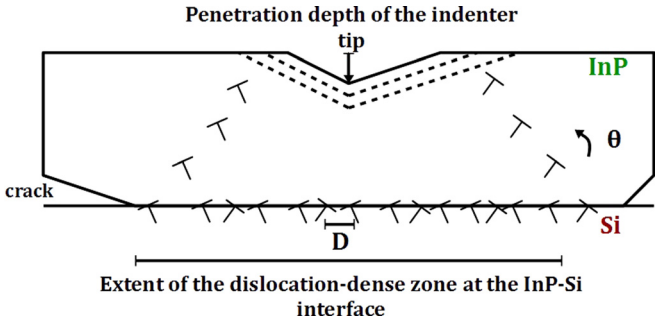

FIG. 6. Schematic illustration of the mechanism responsible for the debonding.

One can take advantage of this phenomenon to compute the surface bonding energy of the bonding interface between the InP membrane and the Si substrate. Indeed, the portion of the InP membrane located within the blister, but outside the dislocation-dense zone surrounding the indenter tip, is elastically deformed. One can thus apply the same formalism as in the crack-opening method to link the debonding crack length to the surface bonding energy. For a given debonding crack length L and a corresponding blister height t_b, the surface bonding energy can be shown to be

$$\gamma = \frac{3E_{\mathrm{InP}}t_{\mathrm{InP}}^3 t_b^2}{16L^4}, \tag{5}$$

where E_{InP} and t_{InP} are the Young modulus and the thickness of the InP membrane, respectively. One should note that, this equation applies only in the case of an elastically debonded InP membrane. Thus, the debonding crack length is not measured from the load center to the crack tip, but from the location of the last dislocation in InP to the crack tip, as shown in the inset of Fig. 2.

Using the debonding crack length and blister height measured on the left-hand side of the BF-STEM image in Figure 2, where the FIB section goes though the middle of the blister, one finds an average surface bonding energy of the oxide-free bonding of InP to Si to be 594 mJ m^{-2}. In this calculation, a Young modulus of 61 GPa (Ref. 20) was used for InP. The calculation was applied to STEM images of the blister for various loads. Except for very low loads (5 mN), where Eq. (5) does not apply, as the rotation is too low and debonding is the result of plastic flow only, the equation yields reasonable values for the surface bonding energy. The results are summarized in Table I. The average surface bonding energy measured for this sample is 585 mJ m^{-2}.

The method presented here may also be useful to compute the surface-bonding energy for other bonding techniques, such as oxide-mediated bonding. Indeed, as the blistering is the result of the indentation by a Berkovich tip, it is expected to occur in the membrane regardless of the bonding technique used. One need not use STEM, which requires special specimen preparation and can prove quite cumbersome to implement, and instead use an atomic force microscope (AFM) or a stylus, or optical, profilometer to evaluate the geometry of the blister. Such an approach offers the additional advantage of providing a means for a statistical analysis of the blisters, by evaluating a higher number of blisters, obtained at the same load. Finally, one should note that the method proposed here provides a highly sensitive and localized measurement of the surface bonding energy, which may provide useful insights as to the origin of wafer-scale bonding inhomogeneities and, ultimately, lead to the optimization of the wafer-bonding procedure used.

The authors would like to gratefully acknowledge funding from the Agence Nationale de la Recherche P2N 2012 grant COHEDIO.

[1]G. Roelkens, J. Brouckaert, D. Taillaert, P. Dumon, R. Notzel, D. Van Thourhout and R. Baets, in *Silicon Photonics*, edited by J. A. Kubby and G. T. Reed, p. K1250 (2006).
[2]Q. Tong and U. Gösele, *Semiconductor Wafer Bonding: Science and Technology*, The ECS Series of Texts and Monographs (Wiley, New York, 1999).
[3]P. Maszara, G. Goetz, A. Caviglia, and J. B. Mckitterick, J. Appl. Phys. **64**, 4943 (1988).
[4]F. Fournel, L. Continni, C. Morales, J. Da Fonseca, H. Moriceau, F. Rieutord, A. Barthelemy, and I. Radu, J. Appl. Phys. **111**, 104907 (2012).
[5]D. Pasquariello and K. Hjort, J. Electrochem. Soc. **147**, 2343 (2000).
[6]Q.-Y. Tong, Q. Gan, G. Hudson, G. Fountain, and P. Enquist, Appl. Phys. Lett. **84**, 732 (2004).
[7]D. Liang, D. C. Chapman, Y. Li, D. C. Oakley, T. Napoleone, P. W. Juodawlkis, C. Brubaker, C. Mann, H. Bar, O. Raday, and J. E. Bowers, Appl. Phys. A: Mater. Sci. Process. **103**, 213 (2011).
[8]A. Talneau, C. Roblin, A. Itawi, O. Mauguin, L. Largeau, G. Beaudouin, I. Sagnes, and G. Patriarche, in *Proceedings of IPRM* (IEEE, 2012), pp. 130–132.
[9]E. Le Bourhis, A. Talneau, I. Sagnes, G. Patriarche, L. Largeau, and D. Troadec, in MRS Proceedings **1510** (2013).
[10]D. Pasquariello, M. Camacho, K. Hjort, L. Dosza, and B. Szentpali, Mater. Sci. Eng., B **80**, 134 (2001).
[11]S. J. Bull, C. R. Mec. **339**, 518 (2011).
[12]P. Chalker, S. Bull, and D. Rickerby, Mater. Sci. Eng., A **140**, 583 (1991).
[13]W. W. Gerberich and M. Cordill, Rep. Prog. Phys. **69**, 2157 (2006).
[14]D. B. Marshall and A. G. Evans, J. Appl. Phys. **56**, 2632 (1984).
[15]C. Rossington, A. G. Evans, D. B. Marshall, and B. T. Khuri-Yakub, J. Appl. Phys. **56**, 2639 (1984).
[16]W. C. Oliver and G. M. Pharr, J. Mater. Res. **7**, 1564 (1992).
[17]D. Kramer, H. Huang, M. Kriese, J. Robach, A. Wright, D. Bahr, and W. W. Gerberich, Acta Mater. **47**, 333 (1998).
[18]M. Hytch, E. Snoeck, and R. Kilaas, Ultramicroscopy **74**, 131 (1998).
[19]J. P. Hirth and J. Lothe, *Theory of Dislocations* (McGraw-Hill, New York, 1982).
[20]N. Nichols, D. Rimai, and R. Sladek, Solid State Commun. **36**, 667 (1980).